Icarus 206 (2010) 104–111

Contents lists available at ScienceDirect

Icarus

journal homepage: www.elsevier.com/locate/icarus

Dayside induced magnetic field in the ionosphere of Mars

F. Akalin [a,*], D.D. Morgan [a], D.A. Gurnett [a], D.L. Kirchner [a], D.A. Brain [b], R. Modolo [c], M.H. Acuña [d,1], J.R. Espley [d]

[a] University of Iowa, Department of Physics and Astronomy, Iowa City, IA 52242, United States
[b] University of California, Berkeley Space Science Laboratory, Berkeley, CA 94720, United States
[c] CETP-IPSL 10-12 Ave de l'Europe, 78140 Vélizy, France
[d] NASA Goddard Space Flight Center, Greenbelt, MD 20071, United States

ARTICLE INFO

Article history:
Received 18 November 2008
Revised 12 March 2009
Accepted 17 March 2009
Available online 20 March 2009

Index terms:
Mars
Magnetic fields
Ionosphere

ABSTRACT

The Mars Advanced Radar for Subsurface and Ionospheric Sounding (MARSIS) onboard the Mars Express spacecraft has occasionally displayed surprising features. One such feature is the occurrence of a series of broadband, low-frequency echoes at equally spaced delay times after the sounder transmitter pulse. The interval between the echoes has been shown to be at the cyclotron period of electrons orbiting in the local magnetic field. The electrons are believed to be accelerated by the large voltages applied to the antenna by the sounder transmitter. Measurements of the period of these "electron cyclotron echoes" provide a simple technique for determining the magnitude of the magnetic field near the spacecraft. These measurements are particularly useful because Mars Express carries no magnetometer, so this is the only method available for measuring the magnetic field magnitude. Using this technique, results are presented showing the large scale structure of the draped field inside the magnetic pile-up boundary. The magnitude of the draped field is shown to vary from about 40 nT at a solar zenith angle of about 25°, to about 25 nT at a solar zenith angle of 90°. The results compare favorably with similar results from the Mars Global Surveyor spacecraft. A fitting technique is developed to derive the vector direction and magnitude of the draped magnetic field in cases where the spacecraft passes through regions with significant variation in the crustal field. The magnetic field directions are consistent with current knowledge of the draping geometry of the magnetic field around Mars.

© 2009 Elsevier Inc. All rights reserved.

1. Introduction

The Mars Advanced Radar for Subsurface and Ionosphere Sounding (MARSIS) onboard the Mars Express spacecraft has provided several unexpected results in it's over three-year period of operation. One such result reported by Gurnett et al. (2005) early in the mission was a series of intense low-frequency echoes, equally spaced in delay time. Assuming that the echoes recur at the local electron cyclotron frequency, the derived magnetic fields were shown to correspond well with the Cain et al. (2003) model of the martian crustal magnetic fields. Based on these observations, Gurnett et al. (2005) proposed that the echoes are produced by bursts of electrons that orbit in the local magnetic field after being accelerated by the large voltages applied to the sounder antenna during the transmit pulse. This model is supported by the observation that the duration of the echoes always correspond to the duration of the sounding pulse, independent of the period of the echoes. Given that this explanation is correct, the period of the echoes can be used to measure the magnitude of the magnetic field. Since there is no magnetometer on Mars Express and since the magnetic field is a fundamental plasma parameter, the ability to measure the magnetic field is potentially of great importance to other investigators studying local plasma effects using the Mars Express data. The purpose of this paper is to explain the methods used to determine the magnetic field magnitude from the period of the electron cyclotron echoes, to show that the technique gives results that are in agreement with magnetic field measurements from other spacecraft in orbit around Mars, and to show how the vector magnetic field can be determined under some circumstances by comparing the measured magnetic field magnitude to existing models of the crustal magnetic field.

The Mars Express spacecraft was launched on June 2, 2003 and inserted into an elliptical orbit around Mars on December 25, 2003. The orbit of Mars Express has a periapsis altitude of about 275 km, an apoapsis altitude of about 10,100 km, and an inclination of 86°. For a more detailed description of Mars Express, see Chicarro et al. (2004).

MARSIS is a low-frequency radar designed to probe the ionosphere, surface, and subsurface of Mars. The instrument consists

* Corresponding author. Address: Department of Physics and Astronomy, University of Iowa, 203 Van Allen Hall, Iowa City, IA 52242, United States.
E-mail address: ferzan-akalin@uiowa.edu (F. Akalin).
[1] Deceased.

0019-1035/$ - see front matter © 2009 Elsevier Inc. All rights reserved.
doi:10.1016/j.icarus.2009.03.021

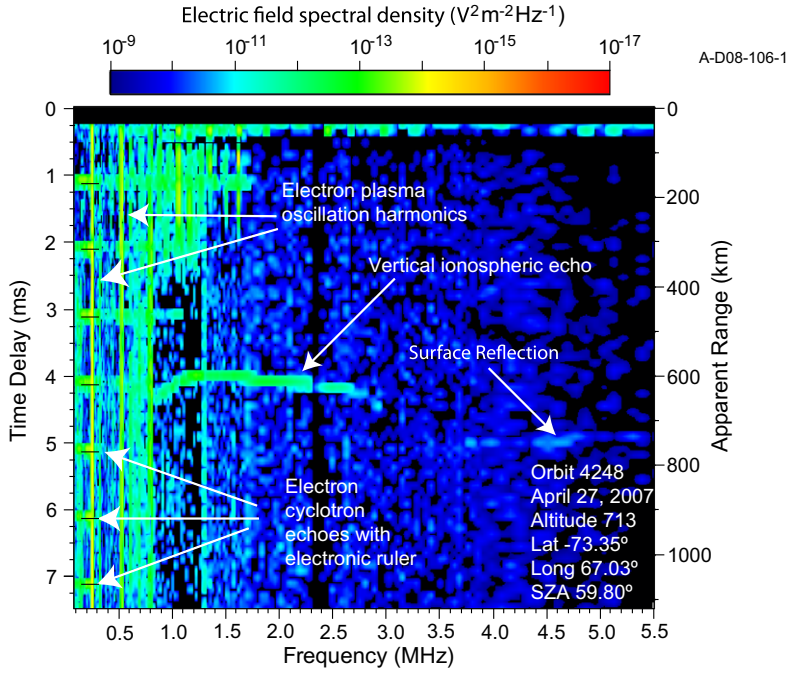

Fig. 1. An ionogram from the dayside of Mars. Frequency is in MHz and is shown along the *x*-axis. Time delay is in ms and is along the *y*-axis. The ionogram shows the electron cyclotron echoes as horizontal bars on the left hand-side. Black marks within the echoes indicate the ticks of an adjustable electronic ruler used to measure the echo spacing. The time between two consecutive echoes is seen to be constant. This time increment is interpreted as the period of the electron cyclotron echoes, and the inverse of this period gives the electron cyclotron frequency. Other features that can be seen in this ionogram are a vertical ionospheric echo, electron plasma oscillation harmonics, and the surface reflection.

of a 40 m electric dipole antenna, a 7 m monopole antenna, a transmitter, a receiver, and a data processing system. The dipole antenna, which is the primary antenna used for ionospheric sounding, was deployed on June 17, 2005, and regular data collection began on July 4, 2005. Collection of ionospheric sounding data usually starts at an inbound altitude of about 1200 km, extends through periapsis at an altitude of about 275 km and ends at an outbound altitude of about 1200 km. A typical ionospheric sounding pass lasts about 40 min. The data analyzed in this paper are from July 30, 2005, to August 8, 2007, and extend over solar zenith angles (SZA) ranging from 0° to 127°. For a more detailed description of MARSIS, see Picardi et al. (2004).

The sounder has two modes of operation: the subsurface mode and the ionospheric sounder mode. The subsurface mode has been used by Picardi et al. (2005) and Plaut et al. (2007) to probe the layer deposits around the martian poles and to search for water and water ice below the martian surface. In this paper we are concerned with the ionospheric sounder mode. This mode is used primarily to probe the ionosphere of Mars and can also detect the surface of the planet. More details and results on the studies using the ionospheric sounder mode can be found in Gurnett et al. (2005, 2008).

The next section of the paper will be dedicated to a discussion of the data, including the appearance and identifying characteristics of the electron cyclotron echoes. We shall discuss the theory of how the echoes are generated and how the magnitude of the magnetic field is computed from these echoes. Statistical results obtained from combining a large number of periapsis passes will be presented to show the structure of the draped interplanetary magnetic field around Mars. It will be shown that results from this technique compare favorably with results from the MGS (Mars Global Surveyor) spacecraft. Finally, a fitting technique will be utilized with individual passes to derive vector components of the magnetic field of the induced draped field of Mars.

First results concerning the magnetic field of Mars, based on magnetic field measurements from the MGS spacecraft, were published by Acuña et al. (1998). The MGS spacecraft had more than 1000 elliptical orbits during its aerobraking and science-phase orbits. After injection into the final circular-mapping orbit, MGS continued to collect data at an altitude of 400 km. The Magnetometer/Electron Reflectometer (MAG/ER) instrument on MGS provided the vector components of the magnetic field of Mars. MARSIS, on the other hand, can only measure the magnitude of the magnetic field. Since Mars Express does not have a magnetometer on board, this technique is the only method of measuring the local magnetic field on Mars Express. Our initial goal in this paper is to (1) introduce a new technique for measuring the magnetic field strength, and (2) compare the results with the magnetic field data from MGS in order to better understand the magnetic field structure of Mars.

2. Description of data and electron cyclotron echoes

The MARSIS ionospheric sounder probes the topside ionosphere of Mars by transmitting a high-intensity, radio frequency pulse, which is then reflected at the level in the ionosphere at which the plasma frequency equals the frequency of the sounding pulse. The highest observed value of the ionospheric plasma frequency is nearly 5.0 MHz (see Gurnett et al., 2008), although values between 2.5 and 4.0 MHz are more typical. If the sounding pulse is higher than the maximum ionospheric plasma frequency, the pulse passes through the ionosphere and is reflected from the surface of Mars. The time between the sounding pulse and the reception of a reflected wave is called the delay time.

The basic visual data product from MARSIS is called an ionogram. A sample ionogram is shown in Fig. 1. Ionograms are produced by transmitting a short pulse at a fixed frequency, f, and measuring the received intensity at 80 consecutive values of the time delay, Δt, spaced 91.4 μs apart. The frequency is then incremented and the process is repeated. For each of 160 frequencies,

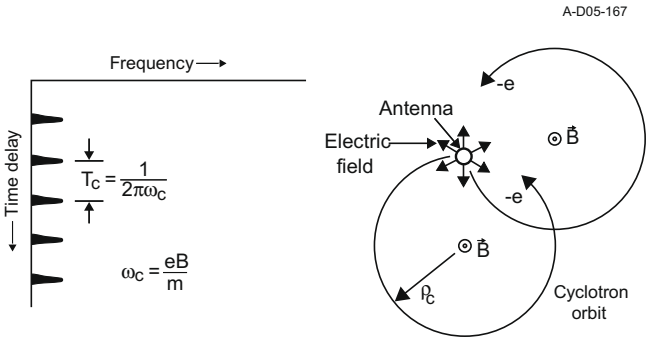

Fig. 2. The generation mechanism of electron cyclotron echoes is shown on the right. The intense voltage pulse on the antenna causes an abrupt acceleration of nearby electrons. These electrons execute cyclotron orbits, returning to the vicinity of the antenna at the electron cyclotron frequency. The appearance of these echoes on ionograms is schematically shown on the left.

quasi-logarithmically spaced between 0.1 and 5.5 MHz, there are 80 delay time bins, spaced 91.4 μs apart, beginning 162.5 μs after the end of the sounding pulse. Ionograms represent received intensity as a function of time delay and frequency. As shown by the ionogram in Fig. 1, time delay is displayed in milliseconds along the vertical axis, frequency is displayed in megahertz along the horizontal axis, and the color bar represents the received electric field spectral density in $V^2\ m^{-2}\ Hz^{-1}$. Ephemeris data such as orbit number, date, altitude in km, latitude, longitude, and solar zenith angle are displayed at the bottom right-hand corner of the ionogram in Fig. 1. Some of the features that are seen on the ionogram are electron cyclotron echoes (see Gurnett et al., 2005, 2008), electron plasma oscillation harmonics (see Duru et al., 2008), vertical ionospheric echoes (see Gurnett et al., 2005, 2008; Morgan et al., 2008) and the surface reflection (see Morgan et al., 2006).

Fig. 2 illustrates how the electron cyclotron echoes are formed. During each cycle of the sounder pulse, a 400 V quasi-sinusoidal pulse is applied to the electric antenna, accelerating nearby electrons. The accelerated electrons execute cyclotron orbits in the local magnetic field. Every time these electrons return to the vicinity of the spacecraft, a short broadband voltage pulse is induced on the antenna, thereby producing the horizontal echoes on the ionogram. The duration of each echo is always approximately the duration of the transmitted pulse, which is 91.4 μs, independent of the local magnetic field strength. The observed echo is usually seen over two time delay intervals because the pulse almost always straddles two such bins. The constant width of the received pulse shows that these electrons travel as a group and that the disturbance is indeed a pulse rather than a wave. Assuming electron energies of 400 eV and magnetic fields between 12 and 160 nT, the radius of the electron cyclotron orbits is between 0.4 and 6.0 km.

For a high-frequency pulse, the electrons near the antenna oscillate at the frequency of the sounding pulse; however, at lower frequencies, electrons travel far enough from the antenna during the negative half cycle that they cannot be drawn back during the following positive half cycle. Thus, the electron cyclotron echoes are seen without exception at low sounding frequencies, typically less than 2 MHz.

It can be seen that the time delays of the individual echoes, as well as the spacing between the echoes, are remarkably constant with respect to frequency. We refer to the time delay spacing as T_c and the corresponding repetition rate as $f_c = 1/T_c$. The magnetic field strength is calculated by assuming that the observed repetition rate is equal to the electron cyclotron frequency, given by the equation $f_c = (1/2\pi)(eB/m_e)$. This equation can be written as $f_c = 28B$ for electrons, where B is the magnitude of the magnetic field in nT, and f_c is given in Hertz (see Gurnett and Bhattacharjee, 2005).

The difference in time delay between the echoes is measured directly on the computer screen by an electronic ruler. This electronic ruler has black tick marks that can be adjusted to align with the electron cyclotron echoes. Once the tick marks are aligned with the echoes, the time delay displayed on the screen is read and recorded as the period of the electron cyclotron echoes. The minimum period between the echoes must be 182.8 μs, or two times the width of a time delay bin, in order for the echoes to be distinguished from each other. The magnetic field corresponding to this period is 195 nT; however, in practice, determining the field when it is greater than 160 nT is difficult. The echoes can be detected unless they are separated in time by more than the maximum detectable delay times of 7.5 ms. The magnetic field corresponding to this period is 5 nT. Thus, the theoretical range of detection of the magnetic field measurements is 5–195 nT. However, in practice we have magnetic field observations from 12 nT up to 160 nT. Assuming a tolerance in the measurements of ±182.8 ms, the uncertainty of the magnetic field measurement is found to be ±2% for the most widely spaced echoes. However, because several echoes can be aligned with the tick marks on the electronic ruler, the cyclotron period can be measured even more accurately.

3. Statistical results

In this section, we analyze the relationship of the measured magnetic field to various orbital quantities such as the spacecraft altitude and solar zenith angle. In doing so, we will compare our results with those of the MGS magnetometer. We will use the results to present a picture of the draped magnetic field on the dayside of Mars.

Data analyzed in this study are from July 30, 2005 to August 8, 2007. MARSIS completed 1037 periapsis passes during this time. We do not account for samples where the magnetic field could not be measured. Because we are attempting to characterize only the draped magnetic field of Mars, crustal field structures must be removed from this combined data set. To achieve this, we selected only data points for which the model of Cain et al. (2003) gives a magnetic field magnitude less than 10 nT at an altitude of 400 km. After eliminating the crustal field structures, approximately 23,000 data points were left. The coverage patterns of these data are similar to these of MGS during aerobraking phase, as shown by Brain, 2007. The principal differences are (1) MARSIS does not sample above 1200 km, (2) MARSIS has better coverage near the subsolar point at low altitudes but does not go beyond a solar zenith angle of 120°, (3) MARSIS sampling is heavily concentrated between 10 and 16 h local time, and (4) MARSIS coverage is weighted toward the southern hemisphere. Fig. 3 shows the contour average of the measured magnetic field, with the contribution of the remnant magnetic field removed, as a function of x and ρ, in units of martian radii. Therefore, Fig. 3 can be interpreted as a map of the draped interplanetary magnetic field. Here, the x-axis is measured along the Mars–Sun line, with $+x$ toward the Sun, and ρ is the distance from the x-axis. The color bar represents the average magnetic field strength in nT. The lines showing the bow shock and the magnetospheric boundary (MB) are from the model of Dubinin et al. (2006), based on electron flux data from Analyzer of Space Plasmas and Energetic Atoms (ASPERA) instrument onboard Mars Express. The MB is sometimes called the magnetic pile-up boundary (MPB), characterized by MGS observations. The magnetic pile-up boundary determined from MGS observations is identified by an increase of the magnitude of the magnetic field, a decrease in electron fluxes and an enhancement of the draping of the magnetic field around the planet (see Bertucci et al., 2003).

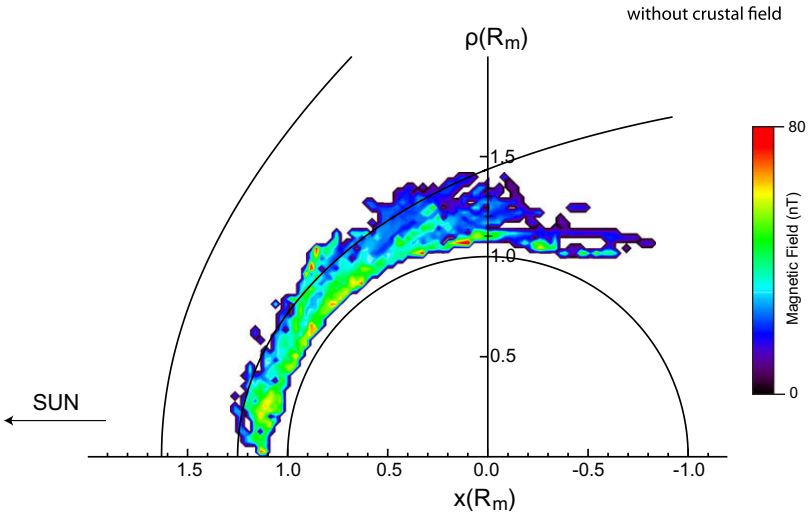

Fig. 3. Distribution of magnetic field strength around Mars, with intense crustal fields removed. The positive horizontal axis is along the Mars–Sun direction. The vertical axis shows ρ, the distance from the Mars–Sun axis. The Sun is to the left. The color bar represents the magnetic field strength in nT. Bow shock and magnetic pile-up boundary are from a model of Dubinin et al. (2006). The measured magnetic field intensity is seen to be at a maximum near the lowest sampled altitudes, decreasing with increasing altitude, and usually undetectable outside the magnetic pile-up boundary.

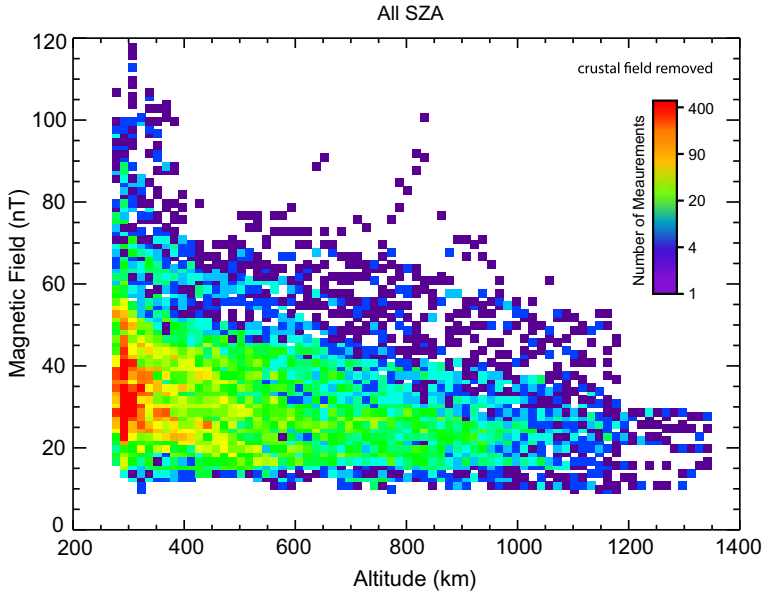

Fig. 4. Distribution of the magnetic field in nT as a function of altitude in km for all sampled solar zenith angles. The number of measurements in each bin is represented by the color bar. Samples near intense crustal field structures have been removed. The most intense magnetic fields are at the lowest altitudes, with the field intensity decreasing consistently with altitude. Some anomalously high fields are noted around 800 km.

Fig. 3 shows that on the dayside of Mars, the magnetic field magnitude is at a maximum at the lowest altitudes sampled, ~275 km, that it decreases with increasing altitude, and that it is generally undetectable outside the MPB. The disappearance of the electron cyclotron echoes outside of the MPB could be due to the following three reasons: first, as mentioned in the previous section, echoes separated by more than 7.5 ms cannot be detected. However, by comparison with Fig. 3 and Fig. 8a of Brain et al., 2003, it is seen that the magnetic field is near the edge of detectability, about 10 nT, at altitudes above the MPB and solar zenith angles greater than 60°. Therefore, we believe that this is unlikely to be the explanation of the lack of observation outside the MPB. A second possibility is that the velocity of the shocked solar wind outside of the MPB is high enough to transport the circulating electron pulses away from the spacecraft before they can be detected. If 10 nT is used as a maximum magnetic field strength inside of the magnetosheath, the electron cyclotron frequency is 280 Hz, implying a cyclotron period of 3.5 ms. If 200 km/s is taken as the velocity of the shocked solar wind, then the maximum electron pulse displacement during one Larmor circle is calculated to be around 700 m, or about 16 times the total length of the antenna. It is plausible, therefore that the shocked solar wind convects these electron pulses out of range of the antenna. A third possibility is that the solar wind just outside of the MPB contains enough turbulence that the electrons do not execute coherent cyclotron orbits.

In Fig. 4 we address the dependence of the magnitude of the draped magnetic field on altitude. This figure shows the distribution of magnetic field magnitude in nT as a function of altitude in km for the same data set used in Fig. 3 but accumulated over all solar zenith angles. The color bar represents the number of mea-

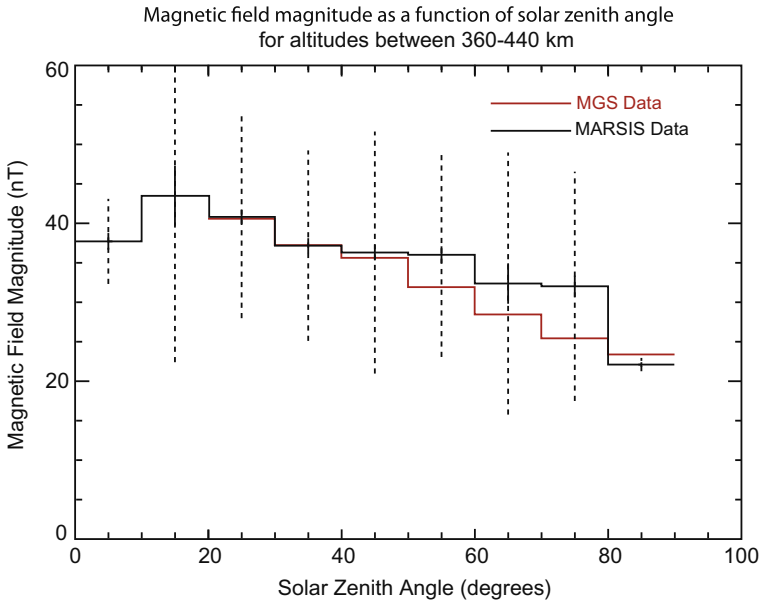

Fig. 5. Magnetic field magnitude in nT as a function of solar zenith angle in degrees. Magnetic field samples are placed in 10° solar zenith angle bins starting at 0°, the subsolar point. The altitude range is restricted to between 360 km and 440 km, since this is where the MARSIS and MAG/ER data sets overlap. Results from MAG/ER (red) and MARSIS (black) are plotted in this histogram. Both distributions indicate a decrease from approximately 45 nT near the subsolar point to 20 nT near the terminator.

surements in each bin, which has dimensions of 12.5 nT by 2 km. The magnitude of the draped interplanetary magnetic field is seen to lie between 10 nT and 120 nT and to steadily decrease as altitude increases from about 275 km to 1000 km. We note some abnormally high magnetic field measurements at altitudes of approximately 800 km. These fields do not reflect structures evident from the Cain et al. (2003) model. We consider it likely that these abnormally high fields represent an interaction of the interplanetary magnetic field with martian crustal fields. This phenomenon is an object of ongoing research.

In Fig. 5 we compare magnetic field magnitude from MARSIS to measurements by the MGS magnetometer. Because Mars Express is in an inertial orbit, it sweeps through a wide range of solar zenith angles including the subsurface point. MGS, on the other hand, orbits in a plane that rotates Sun-synchronously at constant local times of 0200–1400, thus never sampling near the subsolar point. Samples between altitudes of 360 km and 440 km are placed in 10° bins in solar zenith angle, starting at the subsolar point for MARSIS and at 20° for the MGS magnetometer. The histogram in black represents the data points without crustal field from MARSIS and the histogram in red represents the data points without crustal field from the MGS magnetometer. The histogram for the MGS magnetometer is for all measurements taken between September 13, 1998 and November 2, 2006, while the MARSIS data are taken between July 30, 2005 and August 8, 2007. Because we are focusing on the day-side draped field around Mars, we have only plotted both data sets up to a solar zenith angle of 90°. Vertical dashed lines represent the standard deviations of the MARSIS magnetic field magnitudes in each bin. For all but the first and last bins, the MGS magnetometer values are well within the standard deviation of the MARSIS magnetic fields. It should be noted that the MARSIS data were taken over a period of approximately 2 years, comprising a wide variety of solar wind conditions and orbital configurations as well as declining solar activity. These factors should explain the large variation in magnetic field. Although the MGS and MARSIS magnetic field magnitudes agree within the standard deviation of MARSIS measurements over most of the range of solar zenith angle, the values taken by MGS are significantly lower between 50° and 80° solar zenith angle. A plausible explanation for this discrepancy might be that the MGS data were taken at an earlier epoch than the MARSIS data (overlapping only for the final year of operation of MGS) during which solar activity was higher, implying increased ionospheric conductivity and therefore a more efficient screening of the magnetic field. Other explanations might be advanced, citing orbital and epochal idiosyncrasies of the two spacecraft. In any case, the MGS magnetic field measurements between 20° and 80° SZA are clearly within the variation of the MARSIS magnetic field.

We conclude that, in spite of the slightly different sampling epochs, these two data sets are seen to have similar distributions in solar zenith angle. The induced draped field around Mars, as measured by both MARSIS and the MGS magnetometer, has a magnetic field magnitude of approximately 40 nT at a solar zenith angle of 20° which decreases to approximately 25 nT around the terminator. This result confirms that the magnetic environment is sensitive to solar conditions (see Vignes et al., 2000).

4. Determining the vector field

In addition to the statistical results presented in the previous section, we have also carried out a detailed analysis of a few of the periapsis passes in order to determine the vector direction of the draped magnetic field. Fig. 6a shows the MARSIS magnetic field magnitude for the periapsis pass of orbit 4226. Black stars show the MARSIS measurements, and the blue diamonds show the magnetic field magnitude computed from the model of Cain et al. (2003) at the position of the spacecraft. The two measurements track each other very well, with the MARSIS data having higher magnetic fields all along the plot. The model of Cain et al. (2003) gives the crustal fields, based on nightside MGS magnetometer measurements, whereas MARSIS measures the total field, including the draped IMF and the crustal field contribution; therefore, MARSIS measurements are typically higher than those of the Cain et al. (2003). This effect was first noted by Gurnett et al. (2005).

Although MARSIS is only capable of directly measuring the magnitude of the magnetic field, we can, using certain assumptions, compute the direction of the draped magnetic field on the dayside of Mars. The magnetic field magnitude measured by MARSIS, here called B_{marsis}, is the magnitude of the vector sum of the

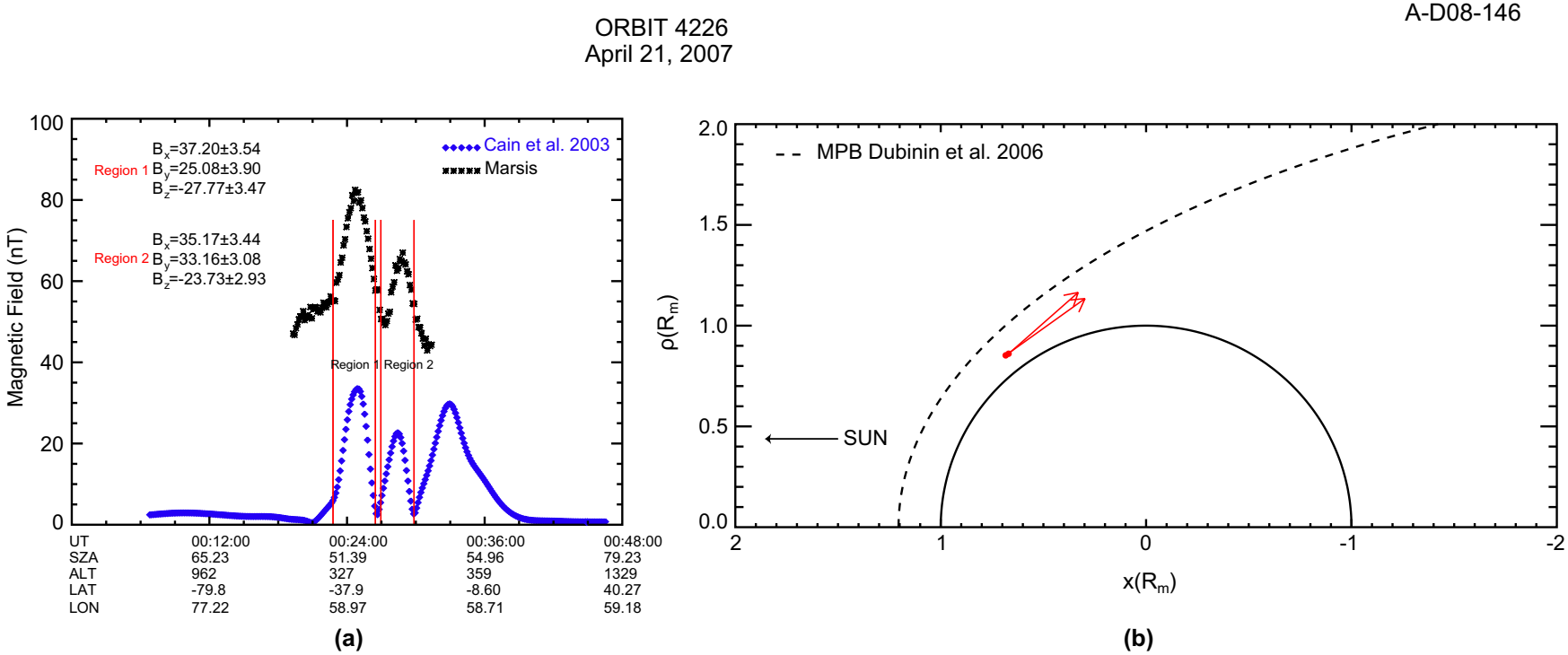

Fig. 6. Extraction of vector draped magnetic field from two segments of orbit 3065. (a) shows the magnetic field magnitude from both MARSIS (black stars) and the crustal field model of Cain et al. (2003) model (blue diamonds) as a function of time. The regions bracketed by vertical red lines are the time intervals used to solve for the vector components of the draped IMF. The numerical results of the fitting procedures are shown on the upper right-hand corner of (a). The resulting vectors are plotted on (b) to illustrate the agreement of the computed draped IMF with the known orientation of the MPB.

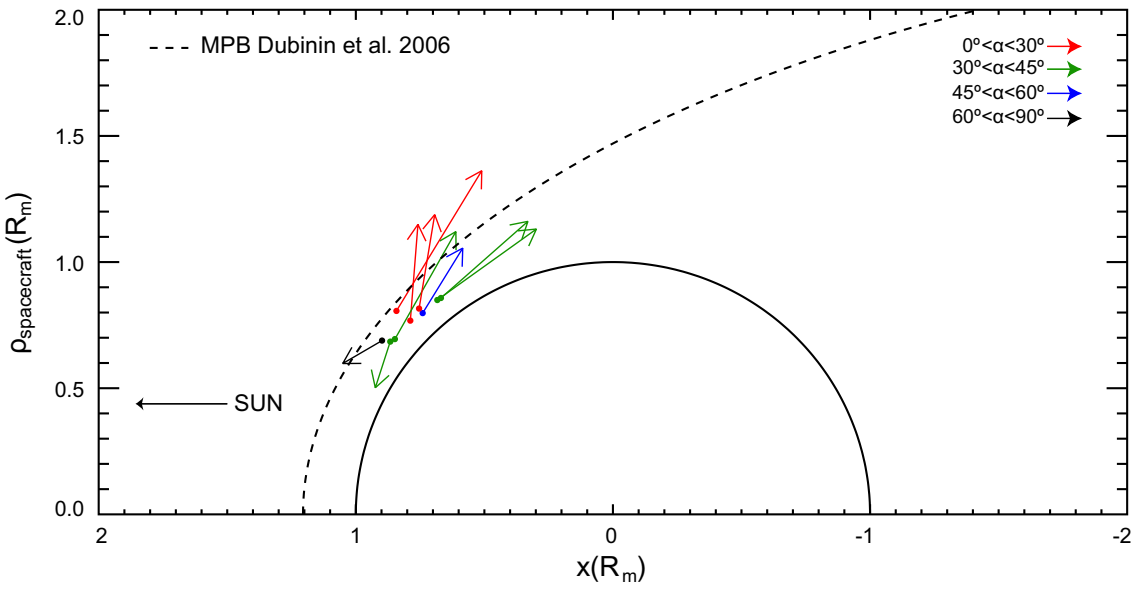

Fig. 7. Results of the method of Section 4 applied to nine time intervals over eight orbits (including results from Fig. 6), for which the angle of uncertainty (as explained in the text) is 5° or less. The x-axis is the Mars–Sun line and the z' axis is chosen so that the x–z' plane contains the Mars-spacecraft vector. Magnetic field results are projected into the x–z' plane. Color coding indicates the out-of-plane angle α of the resulting magnetic field vector. Results suggest the expected draping geometry with some variation.

martian planetary field (given here by the Cain et al., 2003 model), $B_{\text{cain}}^{(r,t)} = [B_{x\_\text{cain}}, B_{y\_\text{cain}}, B_{z\_\text{cain}}]$, and the draped magnetic field, $B_{\text{drp}} = [B_{x\_\text{drp}}, B_{y\_\text{drp}}, B_{z\_\text{drp}}]$, giving the equation

$$B_{\text{marsis}}^{(r,t)} - \left(\left(B_{\text{cain}\_x}^{(r,t)} + B_{x\_\text{drp}} \right)^2 + \left(B_{\text{cain}\_y}^{(r,t)} + B_{y\_\text{drp}} \right)^2 + \left(B_{\text{cain}\_z}^{(r,t)} + B_{z\_\text{drp}} \right)^2 \right)^{1/2} = 0,$$

where we wish to solve for the vector components of B_{drp}. Note that B_{marsis} and B_{cain} are functions of position and time, as Mars Express follows its orbit, whereas B_{drp} is assumed to be constant over the time intervals selected, typically a few minutes in duration. It should be noted that in order to make a reliable fit using this equation, the magnitude of the crustal magnetic field must vary significantly over the selected time and must be significantly different from the total field measured by MARSIS; otherwise, the solution matrix approaches degeneracy. If these conditions are satisfied, the equation given above can be used to compute a least-square fit for the components of B_{drp}. Results of fitting this equation are shown in Fig. 6a.

The region bracketed by the two red lines in Fig. 6a is a time interval that meets the requirements for the fitting procedures. In order to find a unique solution, we vary the x, y, and z components of the IMF over 50 values bracketed by the negative and positive of the maximum values of B_{marsis} for each of the unknown components. For every sample value of the IMF, a normalized squared error is calculated for the combination of vector fields. The solution for the x, y, and z vector of the draped IMF is the one which gives the smallest normalized error. The results of this procedure are plotted in Fig. 6b with the MPB model of Dubinin et al. (2006). The draped IMF observed by MARSIS agrees reasonably well with Fig. 4 of Brain et al. (2003) and also with the expected draped field based on the MPB shape. Thus, we believe this technique to be potentially very useful for determining the vector components of the draped IMF as MARSIS passes over intense crustal fields.

A survey of orbits in which the crustal fields and the magnetic field detected by MARSIS has yielded 15 analyzable intervals during 14 orbits (including the results shown in Fig. 6). The output of the fitting procedure yields uncertainties in all components of the resultant magnetic field. From these uncertainties, we can compute a mean-square error, which can be combined with the resultant magnetic field magnitudes to yield an angle of uncertainty. Fig. 7 shows the nine results for which the angle of uncertainty is 5° or less. The resulting magnetic fields are projected in the x–z' plane for which the x-axis is along the Mars–Sun line and the z'-axis is chosen such that the x–z' plane includes the Mars-spacecraft vector. The color coding indicates the out-of-plane angle for each magnetic field vector. The results of these calculations suggest a tendency for the magnetic field to align itself with the direction of the magnetic pile-up boundary, consistent with the usual concept of a draped field; however, there is a lot of variation about this result. The out-of-plane angle does not appear to organize the results very well. We hope to refine this method and apply it to a variety of cases in the future.

5. Summary

In this paper, we have demonstrated a simple, very accurate technique for measuring the magnetic field around Mars using the MARSIS ionospheric sounder onboard Mars Express, which has no onboard magnetometer. The method has been validated by comparison with results from the MGS magnetometer. We have shown that the magnetic field can be measured on the dayside at altitudes up to the magnetic pile-up boundary. We have detected a clear decrease in the magnitude of the magnetic field of Mars from an average of about 45 nT at a subsolar point of approximately 300 km altitude to below 5 nT, the limit of detectability, near the MPB. The field varies in solar zenith angle from about 40 nT near the subsolar point to about 20 nT near the terminator. The sampling near the subsolar point is from MARSIS only, because of the orbital constraints of MGS.

In addition to statistical results, we have demonstrated a method for extracting the vector components of the draped magnetic field from data intervals of several minutes in which the crustal field is known to vary significantly. We have validated this method by superimposing the resulting vector fields from a sample orbit on the MPB model of Dubinin et al. (2006). Preliminary results of this method suggest significant variability about the expected draping geometry.

In conclusion, the MARSIS ionospheric sounder onboard Mars Express, under certain conditions, can be used as a magnetometer. This is important because Mars Express has no magnetometer, and, as we and others have shown, the magnetic field near Mars can be both variable and dynamic. Knowledge of the magnetic field is a crucial element in the understanding of the ionosphere and space environment near Mars. Indeed, we have noted the existence of numerous instances of anomalously high magnetic fields during the Mars Express mission. We believe that MARSIS magnetic field measurements will provide valuable data in analyzing these and similar occurrences.

Acknowledgments

We would like to acknowledge the contribution of Zeynep Sagtas Bilki to the collection of data for this project. We also thank one of the referees for several insights that helped with our interpretation.

This research was supported by NASA through contract 1224107 with the Jet Propulsion Laboratory.

References

Acuña, M.H., and 19 colleagues, 1998. Magnetic field and plasma observations at Mars: Initial results of the Mars Global Surveyor mission. Science 279, 1676–1680.

Bertucci, C., and 11 colleagues, 2003. Magnetic field draping enhancement at the Martian magnetic pileup boundary from Mars global surveyor observations. Geophys. Res. Lett. 30. doi: 10.1029/2002GL015713.

Brain, D.A., 2007. Mars Global Surveyor measurements of the Martian solar wind interaction. Space Sci. Rev. 126, 77–112. doi: 10.107/s11214-006-9122-x.

Brain, D.A., Bagenal, F., Acuña, M.H., Connerney, J.E.P., 2003. Martian magnetic morphology: Contributions from the solar wind and crust. J. Geophys. Res. 108 (A12), 1424. doi:10.1029/2002JA009482.

Cain, J.C., Ferguson, B.B., Mozzoni, D., 2003. An n = 90 internal potential function of the martian crustal magnetic field. J. Geophys. Res. 108 (E2), 5008. doi:10.1029/2000JE001487.

Chicarro, A., Martin, P., Traunter, R., 2004. The Mars Express mission: An overview. In: Wilson, A. (Ed.), Mars Express: A European Mission to the Red Planet, SP-1240. European Space Agency Publication Division, Noordwijk, Netherlands, pp. 3–16.

Dubinin, E., Fränz, M., Woch, J., Roussos, E., Barabash, S., Lundin, R., Winningham, J.D., Frahm, R.A., Acuña, M., 2006. Plasma morphology at Mars. ASPERA-3 observations. Space Sci. Rev. 126, 209–238. 10.1007/s11214-006-9039-4.

Duru, F., Gurnett, D.A., Morgan, D.D., Modolo, R., Nagy, A.F., Najib, D., 2008. Electron densities in the upper ionosphere of Mars from the excitation of electron plasma oscillations. J. Geophys. Res. 113, A07302. doi:10.1029/2008JA013073.

Gurnett, D.A., Bhattacharjee, A., 2005. Introduction to Plasma Physics with Space and Laboratory Applications. Cambridge Univ. Press, Cambridge, UK.

Gurnett, D.A., and 10 colleagues, 2005. Radar soundings of the ionosphere of Mars. Science 310, 1929–1933.

Gurnett, D.A., and 12 colleagues, 2008. An overview of radar soundings of the Martian ionosphere from the Mars Express spacecraft. Adv. Space Res. 41 (9), 1335–1346. doi: 10.1016/j.asr.2007.01.062.

Morgan, D.D., Gurnett, D.A., Kirchner, D.L., Huff, R.L., Brain, D.A., Boynton, W.V., Acuña, M.H., Plaut, J.J., Picardi, G., 2006. Solar control of radar wave absorption by the Martian ionosphere. Geophys. Res. Lett. 33, L13202. doi:10.1029/2006GL026637.

Morgan, D.D., Gurnett, D.A., Kirchner, D.L., Fox, J.L., Nielsen, E., Plaut, J.J., 2008. Variation of the Martian ionospheric electron density from Mars Express radar soundings. J. Geophys. Res. 113, A09303. doi:10.1029/2008JA013313.

Picardi, G., and 12 colleagues, 2004. MARSIS: Mars advanced radar for subsurface and ionosphere sounding. In: Wilson, A. (Ed.), Mars Express: A European Mission to The Red Planet, SP-1240. European Space Agency Publication Division, Noordwijk, Netherlands, pp. 51–69.

Picardi, G., and 33 colleagues, 2005. Radar soundings of the subsurface of Mars. Science 310, 1925–1928.

Plaut, J.J., and 23 colleagues, 2007. Subsurface radar sounding of the south polar layered deposits of Mars. Science 316, 92–95.

Vignes, D., Mazelle, C., Rème, H., Acuña, M.H., Connerney, J.E.P., Lin, R.P., Mitchell, D.L., Cloutier, P., Crider, D.H., Ness, N.F., 2000. The solar wind interaction with Mars: Locations and shapes of the bow shock and the magnetic pile-up boundary from the observations of the MAG/ER experiment onboard Mars Global Surveyor. Geophys. Res. Lett. 27 (1), 49–52.